PROCEEDINGS OF THE ROYAL SOCIETY A | MATHEMATICAL, PHYSICAL & ENGINEERING SCIENCES

Rotation, inversion and perversion in anisotropic elastic cylindrical tubes and membranes

Alain Goriely and Michael Tabor

Proc. R. Soc. A 2013 **469**, 20130011, published 6 March 2013

PROCEEDINGS OF THE ROYAL SOCIETY A

rspa.royalsocietypublishing.org

Research

Cite this article: Goriely A, Tabor M. 2013 Rotation, inversion and perversion in anisotropic elastic cylindrical tubes and membranes. Proc R Soc A 469: 20130011. http://dx.doi.org/10.1098/rspa.2013.0011

Received: 8 January 2013
Accepted: 8 February 2013

Subject Areas:
applied mathematics, mechanical engineering

Keywords:
nonlinear elasticity, anisotropy, fibre-reinforced, inversion, perversion

Author for correspondence:
Alain Goriely
e-mail: goriely@maths.ox.ac.uk

Rotation, inversion and perversion in anisotropic elastic cylindrical tubes and membranes

Alain Goriely[1] and Michael Tabor[2]

[1]OCCAM, Mathematical Institute, University of Oxford, Oxford, UK
[2]Program in Applied of Mathematics, University of Arizona, Tucson, AZ, USA

Cylindrical tubes and membranes are universal structural elements found in biology and engineering over a wide range of scales. Working in the framework of nonlinear elasticity, we consider the possible deformations of elastic cylindrical shells reinforced by one or two families of fibres. We consider both small and large deformations and the reduction from thick cylindrical shells (tubes) to thin shells (cylindrical membranes). In particular, a number of universal parameter regimes can be identified where the response behaviour of the cylinder is qualitatively different. This include the possibility of inversion of twist or axial strain when the cylinder is subject to internal pressure.

1. Introduction

The natural world abounds with tubular and filamentary structures on many different scales. In the plant kingdom, the wide variety of plant stems, with their differing specialized structures and functions, ranges from the sinuous tendrils of climbing plants [1,2] to the massive trunks of trees [3,4]. In the bacterial kingdom, one finds structures ranging from the tubular unicellular hyphae of actinomycetes [5–7] to the cellular chains found in a strain of *Bacillus subtilis* [8–10]. The fungal kingdom (distinguished from the plant kingdom by its chitin based, as opposed to cellulose based, cell-wall structure) is also rich in hyphal structures with a wide variety of mechanical properties including the powerful penetrative capability of the rice blast fungus [11–13] and the remarkable rotational behaviour of *Phycomyces* [14–21]—one of the central motivations of this paper as elaborated on below. The form and function of all the above can, with varying degrees of verisimilitude, be modelled as cylindrical elastic structures with theoretical constructs ranging from simple geometric descriptions to models involving sophisticated theories of nonlinear elasticity with fibrous reinforcement.

Of particular note, in the context of this paper, is the classic work of Harris & Crofton [22] and Clark & Cowey [23] on the structure of nemertean and turbellarian worms. Building on the concept of a hydrostatic skeleton [24–26] they model the worm body as a cylindrical membrane reinforced with a lattice of crossed, inextensible, fibres winding around the membrane with helical geometry, and they characterize the possible extension and retraction of the lattice network as being analogous to that of lazy tongs or a trellis. Their mathematical model, which is purely geometric, proved to be remarkably successful in explaining their detailed experimental studies of the locomotion and flattening of worms. One of their simplest yet most enduring theoretical results was that for a helical reinforcing fibre of fixed length, the maximum enclosed volume is found at a pitch angle (defined relative to the horizontal in their paper) of $\theta = \tan^{-1}\sqrt{2} \approx 54.74^\circ$. We will refer to the reciprocal of this angle ($\Phi_m = \pi/2 - \theta \approx 35.26^\circ$) as the *magic angle* because it seems to appear, as if by magic, in many different settings. For instance, this angle is believed to be key in understanding the elongation of notochords [27–29]. Further, an inanimate analogue of the model of Clark and Cowey can be found in the McKibben actuator which consists of a flexible tube surrounded by a sheath of braided families of inextensible fibres helically wound in opposing directions. This design is the basis for the so-called pneumatic artificial muscles used in robotics, prosthetics and orthotics [30,31]. These actuators are typically pressure controlled and their precise functionality is determined by the weave of the fibres. As with the Clark and Cowey model the fibre winding angle of 35.26° plays a special role in the actuator design. We will show that the magic angle also appears naturally as a special limiting case of a nonlinear elastic model.

Significant developments in the theory of nonlinear elastic structures with fibrous reinforcements were made by Holzapfel & Ogden [32], Holzapfel & Gasser [33] and Holzapfel *et al.* [34] in their studies of arterial mechanics. In their papers, the artery is modelled as a thick-walled cylindrical tube, representing a non-collagenous matrix reinforced by two layers (the media and adventitia) each of which is composed of two families of collagen fibres wound in a helical configuration about the matrix with the two families wound with opposing orientations. This not only reflects the known structure but also ensures that the model exhibits no torsional moment. Their model introduces new constitutive relations and clearly shows how the hyperelastic free energy needs to be extended by new invariants reflecting the geometry of the reinforcing fibres.

A particular motivation for the current work is the remarkable behaviour of the filamentary fungus *Phycomyces blakesleeanus* that undergoes a series of rotational transitions during aerial growth. During what is known as the Stage IV growth phase, the sporangiophore (the ‘stalk’ of the fungus) extends while rotating in a anti-clockwise manner when viewed from above (Stage IVa) and then, while continuing to grow, spontaneously reverses to a clockwise rotation (Stage IVb). This phase lasts for 24–48 h and is sometimes followed by yet another reversal (Stage IVc) before the overall growth ends. The cell wall of the sporangiophore is, essentially, constructed of chitin microfibrils embedded in an elastic matrix of amorphous material composed of chitosan and chitin. Such a structure naturally lends itself to modelling in terms of an elastic cylinder with helical fibre reinforcements and by using such a model combined with an elastic growth mechanism and theso-called pre-compression of the reinforcing fibres (explained in §2*b*) the authors were able to describe the observed growth and rotational inversions [20].

In order to more fully understand the nature of such spontaneous changes, we investigate, in a more general framework, the values of system parameters and loads where a qualitative change in deformations can occur. For instance, if we consider a capped cylinder under small pressure, we want to determine for which fibre angles and material moduli the cylinder will either increase in length and decrease in radius, or increase in radius and decrease in length. These special values of combined loads and parameters, where such behaviour occurs are referred to as *inversion points* if isolated or *inversion curves* in general and, as described in §6, such inversions can be cast in a rather general framework. Similarly, if we increase the pressure of a capped cylinder and follow the rotation of the cylinder, there may be values for which the rotation viewed as a function of the pressure first increases and then decreases (another example of inversion), and leading eventually to a system where the overall rotation will be right-handed (positive τ) or left-handed (negative τ). This change in handedness is usually referred to as a *perversion* [35], a term introduced by Listing [36] and used by Maxwell [37] to describe the passing of one handedness to another one (a full account of perversion and how it is used in tendrils to create twistless springs can be found in [38]). We will further generalize the notion of inversion and perversion for general systems under loads or remodelling.

2. A mechanical model of an anisotropic tube under pressure

(a) General kinematics

We consider a continuous body whose reference configuration is defined by $\mathcal{B}_0$ with material point position vector $\mathbf{X}$. The body is deformed to the current configuration, $\mathcal{B}$ where the position of a material point $\mathbf{X}$ is $\mathbf{x} = \boldsymbol{\chi}(\mathbf{X}, t)$. The deformation gradient, $\mathbf{F}(\mathbf{X}, t) = \mathrm{Grad}\,\boldsymbol{\chi}$ (taken in the reference configuration), relates a material segment in the reference configuration to the same segment in the current configuration [39]. From the deformation gradient one defines the right and left Cauchy–Green strain tensors

$$\mathbf{C} = \mathbf{F}^{\mathrm{T}}\mathbf{F} \quad \text{and} \quad \mathbf{B} = \mathbf{F}\mathbf{F}^{\mathrm{T}}. \tag{2.1}$$

the invariants of which are

$$I_1 = \mathrm{tr}(\mathbf{C}), \quad I_2 = \tfrac{1}{2}(I_1^2 - \mathrm{tr}(\mathbf{C}^2)) \quad \text{and} \quad I_3 = \det(\mathbf{C}). \tag{2.2}$$

We describe geometrically a field of reinforcement fibres by its direction (unit) vector $\mathbf{M}$ defined at each point $\mathbf{X} \in \mathcal{B}$. Under a deformation $\mathbf{F}$, the vector $\mathbf{M}$ is mapped, in the current configuration, to the vector $\mathbf{m} = \mathbf{F} \cdot \mathbf{M}$. The vector $\mathbf{M}$ can be used to characterize the orientation of a fibre in the material, and as such can be used to model the anisotropic response of a fibre-reinforced isotropic material as demonstrated by Adkins & Rivlin [40], Spencer [41] and Triantafyllidis & Abeyaratne[42]. Rather than describing the general theory (see for instance [43–45]), we specialize our analysis to cylindrical shells allowed to deform by axial and radial extension, twist about their axis and for which the fibres have no radial components. In such a case, there is a class of universal deformations [46] that specify the deformation up to three unknown constants and the semi-inverse problem can be fully solved.

(b) Cylindrical deformations

We now consider a tube of initial inner radius $A = 1$ and outer radius $B > A$, and height H deformed into a tube with radii a and b, and height h. We consider a finite deformation in which the cylinder is allowed to inflate, extend twist while remaining cylindrical at all time. This is the classical inflation–extension–torsion problem of the cylinder for which the deformation reads (in cylindrical coordinates)

$$r = \sqrt{a^2 + \frac{R^2 - A^2}{\zeta}}, \tag{2.3}$$

$$\theta = \Theta + \tau\zeta Z \tag{2.4}$$

and

$$z = \zeta Z, \tag{2.5}$$

so that the position vectors are (respectively),

$$\mathbf{X} = R\mathbf{E}_R + Z\mathbf{E}_Z \tag{2.6}$$

and

$$\mathbf{x} = \lambda R \mathbf{e}_r + \zeta Z \mathbf{e}_z. \tag{2.7}$$

The deformation gradient is thus

$$\mathbf{F} = \operatorname{Grad} \mathbf{x} = \begin{bmatrix} \dfrac{1}{\lambda\zeta} & 0 & 0 \\ 0 & \lambda & \zeta\tau r \\ 0 & 0 & \zeta \end{bmatrix}. \tag{2.8}$$

We will assume that the elastic material is incompressible. Therefore, we can limit our analysis to isochoric deformation for which $\det \mathbf{F} \equiv 1$, i.e. λ is given by

$$\lambda = \frac{r}{R} = \frac{1}{R}\sqrt{a^2 + \frac{R^2 - A^2}{\zeta}}. \tag{2.9}$$

Therefore, a single parameter fully describes the radial profile of the deformation. Setting $\lambda_a = a/A$ it follows that

$$\lambda_b = \frac{b}{B} = \frac{1}{\zeta}\sqrt{1 + \frac{A^2}{B^2}(\zeta\lambda_a^2 - 1)}. \tag{2.10}$$

The anisotropic response of the cylinder is modelled by two families of embedded fibres $\mathbf{M}^{(1)}$ and $\mathbf{M}^{(2)}$. For simplicity, we will refer to a family of distributed fibres simply as *a fibre*. Both fibres wind helically around the axis and may induce a rotation of the cylinder under extension depending on their strengths and angle. In the usual cylindrical coordinate system $(\mathbf{e}_r, \mathbf{e}_\theta, \mathbf{e}_z)$, the components of the direction vectors are

$$\begin{bmatrix} M_r^{(1)} \\ M_\theta^{(1)} \\ M_z^{(1)} \end{bmatrix} = \begin{bmatrix} 0 \\ \cos\Phi \\ \sin\Phi \end{bmatrix} \quad \text{and} \quad \begin{bmatrix} M_r^{(2)} \\ M_\theta^{(2)} \\ M_z^{(2)} \end{bmatrix} = \begin{bmatrix} 0 \\ -\cos\Psi \\ \sin\Psi \end{bmatrix}. \tag{2.11}$$

Here, we have assumed that the fibres remain locally tangent to the cylinder. The angles between the fibres and the circumferential direction are denoted by Φ and Ψ, respectively (figure 1). Note that we have chosen the angle Ψ so that when the angles are equal, $\Phi = \Psi$, the two fibres make the same angle with the axis (we will say the fibres are *opposite*). Under a deformation $\mathbf{F}$, the orientation of the fibre characterized by a vector $\mathbf{M}$ with angle Φ in the reference configuration is mapped, in the current configuration, to the vector

$$\mathbf{m} = \mathbf{F} \cdot \mathbf{M} = \begin{bmatrix} 0 \\ \lambda\cos\Phi + r\zeta\tau\sin\Phi \\ \zeta\sin\Phi \end{bmatrix}. \tag{2.12}$$

Therefore, the new fibre angle is

$$\phi = \arctan\left(\frac{\zeta\sin\Phi}{\lambda\cos\Phi + r\zeta\tau\sin\Phi}\right). \tag{2.13}$$

Because we are interested in demonstrating possible qualitative behaviours of cylinders under loadings, we consider a model of strain-energy function with the simplest possible dependence of both isotropic and anisotropic parts

$$W(I_1, I_4) = W_{\text{iso}}(I_1) + W_{\text{aniso}}(I_4) + W_{\text{aniso}}(I_6), \tag{2.14}$$

where the invariants I_1, I_4, I_6 of the right Cauchy–Green tensor $\mathbf{C} = \mathbf{F}^{\mathrm{T}}\mathbf{F}$ are given by[1]

$$I_1 = \operatorname{tr}\mathbf{C}, \quad I_4 = \mathbf{M}^{(1)} \cdot (\mathbf{C} \cdot \mathbf{M}^{(1)}) \quad \text{and} \quad I_6 = \mathbf{M}^{(2)} \cdot (\mathbf{C} \cdot \mathbf{M}^{(2)}). \tag{2.15}$$

---

[1] We have neglected possible dependence on $I_2 = \frac{1}{2}(I_1^2 - \operatorname{tr}\mathbf{B}^2)$ for the isotropic part and on $I_5 = \mathbf{M}^{(1)} \cdot (\mathbf{C}^2 \cdot \mathbf{M}^{(1)})$ and $I_7 = \mathbf{M}^{(2)} \cdot (\mathbf{C}^2 \cdot \mathbf{M}^{(2)})$, and $I_8 = \mathbf{M}^{(1)} \cdot (\mathbf{C} \cdot \mathbf{M}^{(2)})$ for the anisotropic part.

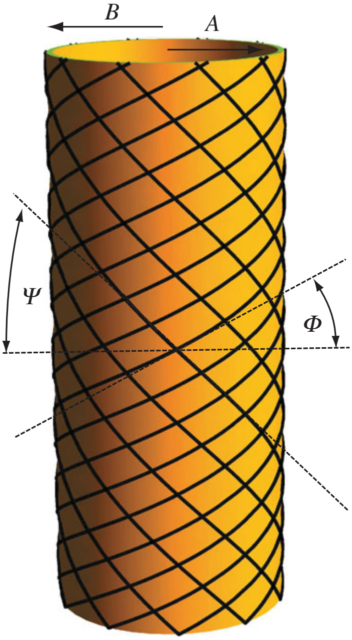

Figure 1. Geometry of the fibres. The angle Φ denote the direction of the first fibre with respect to the cross section (counted anti-clockwise) and the angle Ψ is the angle of the second fibre (counted clockwise). (Online version in colour.)

The invariants I_4, I_6 are the squares of the stretches in the directions of the continuously distributed fibres. Note that $I_4 = \lambda^2 \cos\Phi^2 + \zeta^2 \sin\Phi^2$ so that the fibres are in extension, when $I_4 > 1$, and in compression, when $0 < I_4 < 1$. When $\Phi = 0$, the fibres are aligned with the cross section and $I_4 = \lambda^2$, and when $\Phi = \pi/2$, the fibres are along the axis and $I_4 = \zeta^2$ (figure 1).

We further restrict our attention to simple forms for the isotropic and anisotropic responses in (2.14), the so-called *standard fibre reinforcing model* [42–45,47–49]

$$W_{\text{iso}} = \frac{\mu_1}{2}(I_1 - 3) \tag{2.16}$$

and

$$W_{\text{aniso}}(I_4) = \frac{\mu_4}{4}(I_4 - \nu_1^2)^2 \quad \text{and} \quad W_{\text{aniso}}(I_6) = \frac{\mu_6}{4}(I_6 - \nu_2^2)^2, \tag{2.17}$$

where the material parameters $\mu_i > 0$ have the dimension of a stress (pressure). The parameters ν_i are of particular importance for our problem as they describe the effect of pre-compression (or pre-stretch) of the fibres in the matrix. Fibres can be inserted in the matrix while the matrix is under stress and, as we relax the matrix, the fibres may become compressed or stretched in the reference configuration. Thus, the parameter ν is the stretch needed to put the fibre in its natural length in the reference configuration. For example, if an unstressed fibre is added to an elastic matrix in a state of tension, the fibres in the corresponding reference configuration will be compressed. Hence, the fibre needs to be stretched by a factor $\nu > 1$ to recover its natural length in that reference configuration [48] (see also [50] for an interesting discussion on the connection between this model and the theory of mixtures). Note that for $\nu \neq 1$, the material is residually stressed as even in the absence of external loads, neither the matrix nor the fibres are stress free. This residual stress can be fully computed and naturally influences the state of the system even for small applied loads. As a result non-trivial behaviours can be obtained as we will see in §7 even for very small ν.

From the strain-energy function, we compute the Cauchy stress tensor

$$\mathbf{T} = \mathbf{F}\frac{\partial W}{\partial \mathbf{F}} - p\mathbf{1}, \tag{2.18}$$

where p is the Lagrangian multiplier associated with incompressibility. In our case, the Cauchy stress can be written as

$$\mathbf{T} = 2W_1\mathbf{B} + 2W_4\mathbf{m}^{(1)} \otimes \mathbf{m}^{(1)} + 2W_6\mathbf{m}^{(2)} \otimes \mathbf{m}^{(2)} - p\mathbf{1}, \tag{2.19}$$

with $W_i = \partial_{I_i} W$.

(c) Boundary conditions

We consider a simple thought experiment in which the tube is capped at both ends and subject to an axial extension ζ owing to an internal pressure P and to a total axial load N on the top cap. The tube is also subject to an external moment M leading to a torsion represented by τ. Taking $\mathbf{T}_{rr}(r = b) = 0$, the two first boundary conditions associated with the loads are

$$\mathbf{T}_{rr}(r = a) = -P, \quad \mathbf{T}_{rr}(r = b) = 0 \tag{2.20}$$

and

$$\mathbf{T}_{zz}(z = 0) = N_z, \quad \mathbf{T}_{zz}(z = h) = N_z, \tag{2.21}$$

The first condition relates the radial stress to the pressure jump across the tube wall. The second condition corresponds to the combination of an external axial stress superimposed on the point-wise stress owing to the internal pressure acting on the end cap (we assume, for instance, that the tube is capped by a half sphere of the same thickness as the tube). We now replace these point-wise conditions by integral conditions relating the total application of forces and moments on the faces of the cylinder.

First, we note that the Cauchy equation $\mathrm{div}\mathbf{T} = 0$ leads to a single equation

$$\frac{\mathrm{d}T_{rr}}{\mathrm{d}r} + \frac{1}{r}(T_{rr} - T_{\theta\theta}) = 0. \tag{2.22}$$

This equation can be integrated once over r

$$T_{rr}(r) = \int_r^b \frac{T_{rr} - T_{\theta\theta}}{r}\,\mathrm{d}r, \quad a \le r \le b \tag{2.23}$$

and at $r = a$, the first boundary condition can be replaced by

$$P = \int_a^b \frac{T_{\theta\theta} - T_{rr}}{r}\,\mathrm{d}r. \tag{2.24}$$

Second, even in the absence of torsion ($\tau = 0$), it is well known [51,52] that these conditions cannot be satisfied exactly within the set of allowed deformations given by (2.3). The problem stems from the fact that a constant axial stretch ζ cannot be used to fit a constant N_z because an explicit computation reveals that the axial stress T_{zz} depends on r. The classical solution to this problem is, for long enough tubes, to replace the local point-wise condition by an integral condition for the total axial load applied on the cap

$$2\pi \int_a^b T_{zz} r\,\mathrm{d}r = N = F + \chi P\pi a^2, \tag{2.25}$$

where $N = 2\pi \int_a^b N_z r\,\mathrm{d}r$, thereby eliminating the explicit dependence on the variable r. The total axial load N is further decomposed into an external applied load F (pulling or compressing the tube) and the load created by the internal pressure acting over the cap (pressure times projected area of the cap), the coefficient $\chi = 1$ for a capped cylinder and $\chi = 0$ for an infinite cylinder. For an incompressible material, this last expression is not the most practical one as the term

T_{zz} will contain an arbitrary pressure. An equivalent expression can be obtained by adding and subtracting T_{rr}

$$2\pi \int_a^b T_{zz} r \,\mathrm{d}r = 2\pi \int_a^b (T_{zz} - T_{rr} + T_{rr}) r \,\mathrm{d}r. \tag{2.26}$$

The last term can be integrated by parts, and use of the balance law (2.22) gives

$$2\pi \int_a^b T_{zz} r \,\mathrm{d}r = \pi \int_a^b (2T_{zz} - T_{rr} - T_{\theta\theta}) r \,\mathrm{d}r + P\pi a^2, \tag{2.27}$$

which implies

$$\pi \int_a^b (2T_{zz} - T_{rr} - T_{\theta\theta}) r \,\mathrm{d}r = F + (\chi - 1) P\pi a^2, \tag{2.28}$$

and the last term vanishes for a capped cylinder, the case considered here.

Third, when $\tau \neq 0$, we have to take into account the possibility of applying a moment on the ends. This loading can be expressed also as an integral condition relating the total moment acting on the tube axis to the axial stress. That is,

$$\int_a^b T_{\theta z} r^2 \,\mathrm{d}r = M. \tag{2.29}$$

Therefore, the three boundary conditions for long thin tubes are:

$$C_1: \quad \int_a^b \frac{T_{\theta\theta} - T_{rr}}{r} \,\mathrm{d}r = P, \tag{2.30}$$

$$C_2: \quad \pi \int_a^b (2T_{zz} - T_{rr} - T_{\theta\theta}) r \,\mathrm{d}r = F \tag{2.31}$$

and

$$C_3: \quad 2\pi \int_a^b T_{\theta z} r^2 \,\mathrm{d}r = M. \tag{2.32}$$

The semi-inverse problem consists in finding the values of (λ_a, ζ, τ) corresponding to the three external loads (F, M, P) through the analysis of equilibria.

3. Analysis of equilibria

The non-vanishing components of the Cauchy stress tensor given by (2.19) are

$$T_{rr} = -p + 2W_1 \zeta^{-2} \lambda^{-2}, \tag{3.1}$$

$$\begin{aligned} T_{\theta\theta} = -p &+ 2(\lambda^2 + r^2\zeta^2\tau^2) W_1 \\ &+ 2(\lambda \cos \Phi + r\zeta\tau \sin \Phi)^2 W_4 - 2(\lambda \cos \Psi - r\zeta\tau \sin \Psi)^2 W_6, \end{aligned} \tag{3.2}$$

$$T_{zz} = -p + 2\zeta^2 W_1 + 2\zeta^2 \sin \Phi^2 W_4 + 2\zeta^2 \sin \Psi^2 W_6 \tag{3.3}$$

and

$$\begin{aligned} T_{z\theta} = T_{\theta z} = 2\zeta [&r\zeta\tau W_1 + \sin \Phi (\lambda \cos \Phi + r\zeta\tau \sin \Phi) W_4 \\ &- \sin \Psi (\lambda \cos \Psi - r\zeta\tau \sin \Psi) W_6]. \end{aligned} \tag{3.4}$$

Because the constitutive relationships are written in terms of λ, ζ, τ, we rewrite the three boundary conditions in terms of λ using the identity

$$\frac{\mathrm{d}r}{\mathrm{d}\lambda} = A \frac{(1 - \zeta\lambda_a^2)^{1/2}}{(1 - \zeta\lambda^2)^{3/2}}, \tag{3.5}$$

which yields the equivalent boundary conditions

$$C_1: \quad \int_{\lambda_a}^{\lambda_b} \frac{T_{rr}-T_{\theta\theta}}{\lambda(\lambda^2\zeta-1)}\,\mathrm{d}\lambda = P, \tag{3.6}$$

$$C_2: \quad \pi A^2 \int_{\lambda_a}^{\lambda_b} \frac{1-\zeta\lambda_a^2}{(1-\zeta\lambda^2)^2}\lambda(2T_{zz}-T_{rr}-T_{\theta\theta})\,\mathrm{d}\lambda = F \tag{3.7}$$

and

$$C_3: \quad 2\pi A^3 \int_{\lambda_a}^{\lambda_b} \frac{(1-\zeta\lambda_a^2)^{3/2}}{(1-\zeta\lambda^2)^{5/2}}\lambda^2 T_{z\theta}\,\mathrm{d}\lambda = M. \tag{3.8}$$

While explicit expression for the three integrals for $(M, N$ and $P)$ for the particular choice (2.16) and (2.17) can be obtained, they are far too cumbersome to be useful.

4. Membrane limit

We can take advantage of the assumption that the tube is thin and expand $(M, N$ and $P)$ in the thickness of the tube. Without loss of generality, we measure all lengths with respect to the inner reference radius, that is we set $A = 1$. Then, we introduce ϵ by $B = 1 + \epsilon$ and expand

$$M = M^{(1)}\epsilon + M^{(2)}\epsilon^2 + \ldots, \quad F = F^{(1)}\epsilon + F^{(2)}\epsilon^2 + \ldots \quad \text{and} \quad P = P^{(1)}\epsilon + P^{(2)}\epsilon^2 + \cdots. \tag{4.1}$$

Explicitly, to first order these expressions read

$$\begin{aligned} M^{(1)} &= 2\pi\lambda[\zeta\lambda\mu_1\tau + \mu_4 J_4 \sin(\Phi)(\zeta\lambda\tau\sin(\Phi) + \lambda\cos(\Phi)) \\ &\quad + \mu_6 J_6 \sin(\Psi)(\zeta\lambda\tau\sin(\Psi) - \lambda\cos(\Psi))], \end{aligned} \tag{4.2}$$

$$\begin{aligned} F^{(1)} &= -\frac{\pi}{\zeta}\left[\frac{\mu_1}{\zeta^2\lambda^2}(1 + \zeta^4\lambda^2(\lambda^2\tau^2 - 2) + \zeta^2\lambda^4)\right. \\ &\quad + \mu_4 J_4(\zeta\sin(\Phi)(\zeta(\lambda^2\tau^2 - 2)\sin(\Phi) + 2\lambda^2\tau\cos(\Phi)) + \lambda^2\cos^2(\Phi)) \\ &\quad \left. + \mu_6 J_6(\zeta^2(\lambda^2\tau^2 - 2)\sin^2(\Psi) - 2\zeta\lambda^2\tau\sin(\Psi)\cos(\Psi) + \lambda^2\cos^2(\Psi))\right] \end{aligned} \tag{4.3}$$

and

$$\begin{aligned} P^{(1)} &= \frac{1}{\zeta}\left[\frac{\mu_1}{\zeta^2\lambda^4}(\zeta^4\lambda^4\tau^2 + \zeta^2\lambda^4 - 1)\right. \\ &\quad \left. + \mu_4 J_4(\zeta\tau\sin(\Phi) + \cos(\Phi))^2 + \mu_6 J_6(\cos(\Psi) - \zeta\tau\sin(\Psi))^2\right], \end{aligned} \tag{4.4}$$

where

$$J_4 = (I_4 - \nu_1^2) = \zeta\sin(\Phi)(\zeta(\lambda^2\tau^2 + 1)\sin(\Phi) + 2\lambda^2\tau\cos(\Phi)) + \lambda^2\cos^2(\Phi) - \nu_1^2 \tag{4.5}$$

and

$$J_6 = (I_6 - \nu_2^2) = \zeta^2(\lambda^2\tau^2 + 1)\sin^2(\Psi) - 2\zeta\lambda^2\tau\sin(\Psi)\cos(\Psi) + \lambda^2\cos^2(\Psi) - \nu_2^2. \tag{4.6}$$

For the remainder of this paper, we will work in the membrane limit. Therefore, we drop the superscript $^{(1)}$ in the previous expression and use instead (M, F, P) to denote the applied loads.

5. Inversions and perversions

We are interested in finding values of the parameters and the loads where a qualitative change in some components of the displacement occurs. When we follow the behaviour of the structure under a continuous change of loads for fixed material parameters, we refer to this as following a *loading path*. It is not too difficult to envisage a laboratory experiment in which such a path can be realized, e.g. following the radial and axial strains of a capped cylinder as a function of increasing pressure. When we follow the behaviour of the structure as a function of material parameters, for fixed loads, we refer to this as following a *remodelling path*. Although it is difficult to imagine a laboratory experiment in this case, it might well be realized in Nature, e.g. in a growing plant in

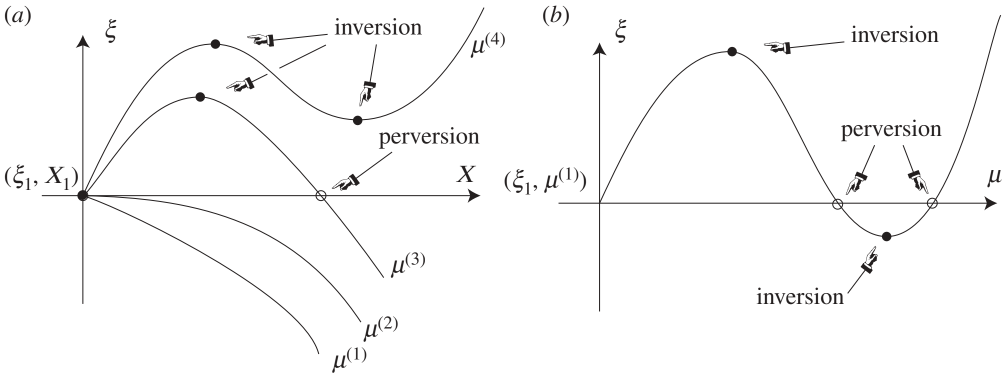

Figure 2. (*a*) Sketch of possible inversions and perversions for different values of a parameter μ under loading. The different values $\mu^{(i)}$, $i = 1, 2, 3, 4$ should not be confused with the parameters in the elastic energy. (*b*) Inversion and perversion under remodelling: a remodelling path at fixed load but varying parameters. (*a*) At $\mu = \mu^{(2)}$ the slope at the origin vanishes, and in a remodelling path going from $\mu^{(1)}$ to $\mu^{(3)}$ and passing through $\mu^{(2)}$ the point (ξ_1, X_1) at $\mu = \mu^{(2)}$ is also an inversion point.

which the orientation (and strength) of the fibres reinforcing the cell wall change continuously during the growth process. It also corresponds to the study of similar structures with slightly different material parameters. For instance, we could consider pressurizing a series of identical cylindrical tubes with slightly different fibre orientation and compare their behaviour under the same loads.

For either type of path we will distinguish between two types of qualitative change. If a strain passes through a maximum or minimum, we will refer to this as an *inversion point*. Around this point, the strain will be non-monotonous. If a strain passes through a special value that results in a particular change in displacement we will refer to this as a *perversion point*. For example, there can be material anisotropies for which the torsion spontaneously changes sign (i.e. the value of the torsion passes through zero) resulting in a change in rotation from clockwise to anti-clockwise, or vice versa. For clarity, we will sometimes refer to this as rotational perversion. For reasons that will become apparent shortly it is useful to extend the notion of perversion to axial and radial strains when they pass through the value of unity—a passage that represents a change from expansion to shrinkage, or vice versa relative to a reference state.

These concepts are illustrated in the sketch in figure 2, where we first consider inversion and perversion under loading. Here, a strain ξ is plotted as a function of a load X for various values of a material parameter μ.[2] We start with an initial state (ξ_1, X_1). For $\mu = \mu^{(1)}$, there is no inversion, and the strain is monotonous with respect to the load. For $\mu = \mu^{(3)}$, the system has one inversion point and one perversion point: if one follows the system under the load X from the initial state, the strain goes through a maximum, (i.e. an inversion point), then passes through a special critical value, i.e. a perversion point (e.g. if ξ represents torsion, this would correspond to $\xi = 0$).The curve corresponding to $\mu = \mu^{(4)}$ illustrates the situation of multiple inversions but no perversion. Similarly, inversion and perversion can also occur in remodelling. In this scenario, shown in figure 2*b*, all loads are fixed and the question is to determine the particular values of a material parameter, say μ, at which the system exhibits either inversions or perversions.

One can also consider inversion under loading owing to a change of parameters. The different curves in figure 2*a* correspond to different material parameters, and changing μ from $\mu^{(1)}$ to $\mu^{(4)}$ corresponds to remodelling the system. At $X = X_1$, the parameter value $\mu^{(2)}$ gives an inversion point yet the local behaviour of the system when the load is slightly varied, for parameter values below and above $\mu^{(2)}$, is qualitatively different because the strain changes sign at $\mu = \mu^{(2)}$.

We also note that according to our definitions of inversion and perversion, it is possible for an inversion point to be associated with a perversion if the inversion point coincides with a

---

[2] This parameter could be any material parameter, not just the moduli used in the previous section.

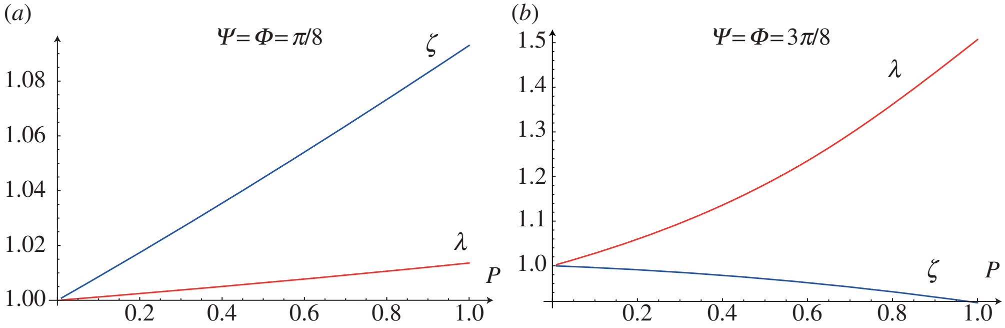

Figure 3. Possible behaviours for the axial and radial strain for a tube with equal and opposite fibres. (*a*) For low angles the tube tends to increase in length, (*b*) for high angles, the tube tends to increase in girth ($\mu_1 = 1$, $\mu_4 = \mu_6 = 10$ and $\nu_1 = \nu_2 = 1$). (Online version in colour.)

strain value that we associate with a perversion behaviour, e.g. the point $\tau = 0$. For clarity we will sometimes refer to a perversion as a *true perversion*, if it does not correspond to a critical point in the strain.

Overall, depending on the chosen path a wide range of behaviours is possible. Before presenting our general theory of inversions, we consider two contrasting illustrative examples.

(a) A tube with equal and opposite fibres under loading

We consider the case of a tube with symmetrically crossed fibres and follow a loading path in which the pressure is increased. The results (figure 3) are intuitive: with fibre angle $\phi = \psi = \pi/8$ the fibres are predominantly providing hoop reinforcement to the tube and, as the pressure is increased, it is much easier for the tube to extend (ζ grows steadily) than to expand (λ increases very slowly). By contrast the case of $\phi = \psi = 3\pi/8$ corresponds to an effective axial reinforcement and it is much easier for the tube to expand (λ grows steadily) than extend (now ζ decreases as a function of increasing pressure). In both cases, we see neither inversion or perversion points. However, the two behaviours are qualitatively different. Therefore, we expect that there is a particular value of the angle $\phi_{\mathrm{cr}} = \psi_{\mathrm{cr}}$ for which the tube inverts its behaviour from extending to inflating. In a remodelling path, where both angles are changed simultaneously (while keeping all loads and the material parameters constant), this particular angle ϕ_{cr} is an inversion point. These cases will be explored in detail in the next section.

(b) A tube with equal fibres at different angles under remodelling

Next, we consider a remodelling path in which one fibre has a fixed angle (say $\Psi = \pi/4$) and, for a fixed pressure, the other fibre orientation, Φ, is increased from 0 to π (figure 4). If the fibre angles are not equal (and there is no external moment), the cylinder will rotate to release the angular stress. The plot of τ as a function of Φ shows two (true) perversion points: the obvious one at $\Phi = \Psi$ and one at $\Phi = 0.4726\ldots$. The appearance of this second perversion point is not difficult to rationalize on physical grounds, but determining the value of Φ at which it occurs requires the theory given below. The τ–Φ plot also shows four inversion points (two minima and two maxima). The behaviour of the extensional strain, ζ, is particularly rich: we see four perversion points (passage through $\zeta = 1$ and four inversion points. By contrast, the radial strain, λ, displays four inversion points but no perversions ($\lambda > 1$ for all Φ).

6. A general theory of inversion along a loading path

We consider a general mechanical system for which a family of deformations is known for given applied loads. Let $\mathbf{X} \in \mathbb{R}^n$ be a vector of loads, and let $\boldsymbol{\xi} \in \mathbb{R}^n$ be the associated generalized strains

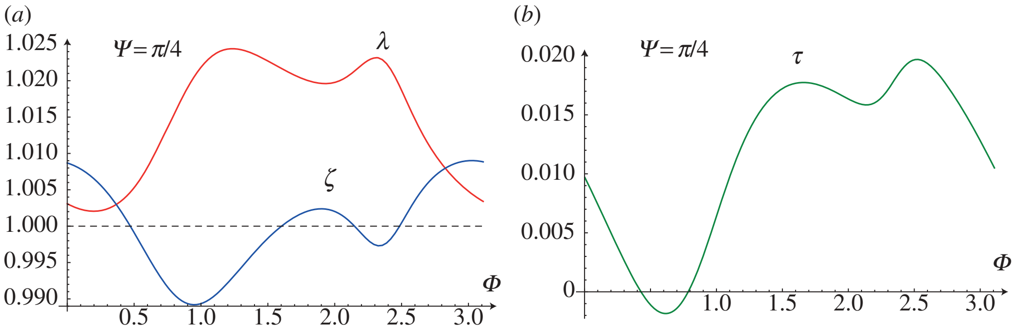

Figure 4. (*a*,*b*) Possible behaviours for the axial and radial strains for a tube with fibres with equal strength, but different orientation. We fix one fibre angle and vary the second one. Along this *remodelling path*, we observe a series of inversions and perversions for the axial strains and the torsion ($\mu_1 = 1$, $\mu_4 = \mu_6 = 10$, $\nu_1 = \nu_2 = 1$ and $P = 0.1$). (Online version in colour.)

or displacements.[3] We assume that there is a sufficiently smooth relationship between the loads and the strains of the form

$$\mathbf{X} = \mathbf{f}(\boldsymbol{\xi}; \boldsymbol{\mu}), \tag{6.1}$$

which fully determines the mechanical problem. Here $\boldsymbol{\mu} = (\mu_1, \mu_2, \ldots, \mu_m)$ is a vector of parameters.

We consider a loading path, namely a particular one-parameter family of loading corresponding to a non-intersecting smooth path $\mathbf{X} = \mathbf{X}(s)$ in $\mathbf{X}$-space parametrized by a variable $s \in [s_1, s_2]$. We assume that no bifurcation occurs in the interval (see the explicit condition below). For a given base value of $s = s^* \in [s_1, s_2]$, we have a corresponding pair $(\boldsymbol{\xi}^*, \mathbf{X}^*) = \mathbf{f}(\boldsymbol{\xi}^*; \boldsymbol{\mu})$. Close to this point, we consider general variations of the strains with respect to the load. Therefore, for small load increments, we have

$$\boldsymbol{\xi} = \boldsymbol{\xi}^* + \mathbf{A}(\boldsymbol{\xi}^*, \boldsymbol{\mu}) \cdot (\mathbf{X} - \mathbf{X}^*), \tag{6.2}$$

where $\mathbf{A}$ is the inverse of the Jacobian matrix of $\mathbf{f}$ evaluated at s^*, that is

$$\mathbf{A} \equiv \left(\left. \frac{\partial \mathbf{f}(\boldsymbol{\xi}; \boldsymbol{\mu})}{\partial \boldsymbol{\xi}} \right|_{\mathbf{X}=\mathbf{X}^*} \right)^{-1}. \tag{6.3}$$

A bifurcation occurs when the matrix $\mathbf{A}$ has a non-empty null-space. Since we assume that no bifurcation occurs in $[s_1, s_2]$, the matrix $\mathbf{A}$ is well-defined. As it stands, (6.2) is simply a linearization of the mechanics about a given reference state.

The system (6.2) can now be used to provide a criterion for predicting inversions. The tangent along the loading path at any point s is given by

$$\mathbf{V}(s) = \frac{\partial \mathbf{X}}{\partial s}, \tag{6.4}$$

and, in particular, at $s = s^*$, $\mathbf{V}^* = \mathbf{V}(s^*)$. The corresponding strain increment, $\mathbf{v}^*$, is simply given by

$$\mathbf{v}^* = \mathbf{A}(\boldsymbol{\xi}^*, \boldsymbol{\mu}) \cdot \mathbf{V}^*. \tag{6.5}$$

We define an *inversion* (*under loading*) in the strain ξ_i at a base state $(\boldsymbol{\xi}^*, \mathbf{X}^*)$ as an extremum along the loading path. Explicitly, this is defined by the conditions

$$v_i^* = 0 \quad \text{and} \quad \left. \frac{\partial^k v_i}{\partial s^k} \right|_{s=s^*} \neq 0, \tag{6.6}$$

---

[3] By generalized strains we include all possible convenient characterizations of a deformation such as displacements and/or stretches.

for at least one component i and an odd number k. Note that v_i^* cannot vanish identically for all i, otherwise $(\boldsymbol{\xi}^*, \mathbf{X}^*)$ would be a bifurcation point. The condition $v_i^* = 0$ is given by

$$\sum_{j=1}^{n} A_{ij}(\boldsymbol{\xi}^*, \boldsymbol{\mu}) \cdot V_j^* = 0, \tag{6.7}$$

that, in turn, provides a condition on the parameters $\boldsymbol{\mu}$.

In the case where we are interested in the change of a strain with respect to a single load, we denote by

$$\mathcal{C}(\xi_i \mid X_j) = A_{ij} = 0, \tag{6.8}$$

the condition for an inversion of strain ξ_i owing to a change in the load X_j.

(a) Application to the cylindrical membrane problem

In our problem, we have three loads[4] $X_1 = P,\ X_2 = F$ and $X_3 = M$ with associated strains $\xi_1 = \lambda$, $\xi_2 = \zeta$ and $\xi_3 = \tau$. Our vector of parameters is $\boldsymbol{\mu} = \{\mu_1, \mu_4, \mu_6, \nu_1, \nu_2, \Phi, \Psi\}$. The associated load–displacement function $\mathbf{f}$ is given by the three equations (4.2)–(4.4). We first restrict our attention to loads close to the reference configuration, that is we choose the base state $\mathbf{X}^* = \mathbf{0}$ and $\boldsymbol{\xi}^* = (1, 1, 0)$. In this case, the matrix $\mathbf{A}^{-1}$ is, in components,

$$\begin{aligned}
(\mathbf{A}^{-1})_{11} &= 2\mu_1 + 2(\mu_4 \cos^4(\Phi) + \mu_6 \cos^4(\Psi)),\\
(\mathbf{A}^{-1})_{12} &= 2\mu_1 - \mu_4 \cos^2(\Phi)(\cos(2\Phi) - \nu_1^2) + \mu_6 \cos^2(\Psi)(\nu_2^2 - \cos(2\Psi)),\\
(\mathbf{A}^{-1})_{13} &= \frac{1}{2}\mu_4 \sin(2\Phi)(3 - 2\nu_1^2 + \cos(2\Phi)) - \frac{1}{2}\mu_6 \sin(2\Psi)(3 - 2\nu_2^2 + \cos(2\Psi)),\\
(\mathbf{A}^{-1})_{21} &= \mu_4\pi \cos^2(\Phi)(2\nu_1^2 - 3\cos(2\Phi) - 1) + \mu_6\pi \cos^2(\Psi)(1 - 2\nu_2^2 + 3\cos(2\Psi)),\\
(\mathbf{A}^{-1})_{22} &= 6\mu_1\pi + \frac{\pi}{4}(\mu_4(2\nu_1^2(\cos(2\Phi) - 3) - 10\cos(2\Phi) + 3\cos(4\Phi) + 11)\\
&\quad + \mu_6(2\nu_2^2(\cos(2\Psi) - 3) - 10\cos(2\Psi) + 3\cos(4\Psi) + 11)),\\
(\mathbf{A}^{-1})_{23} &= \frac{\pi}{2}\mu_6 \sin(2\Psi)(1 - 2\nu_2^2 + 3\cos(2\Psi)) - \frac{\pi}{2}\mu_4 \sin(2\Phi)(1 - 2\nu_1^2 + 3\cos(2\Phi)),\\
(\mathbf{A}^{-1})_{31} &= \frac{\pi}{2}\mu_4 \sin(2\Phi)(3 - 2\nu_1^2 + \cos(2\Phi)) - \frac{\pi}{2}\mu_6 \sin(2\Psi)(3 - 2\nu_2^2 + \cos(2\Psi)),\\
(\mathbf{A}^{-1})_{32} &= 4\pi(\mu_4 \sin^3(\Phi)\cos(\Phi) - \mu_6 \sin^3(\Psi)\cos(\Psi))\\
\text{and}\quad (\mathbf{A}^{-1})_{33} &= 2\pi\mu_1 + 2\pi\mu_4 \sin^2(\Phi)(2 - \nu_1^2 + \cos(2\Phi)) + 2\pi\mu_6 \sin^2(\Psi)(2 - \nu_2^2 + \cos(2\Psi)).
\end{aligned} \tag{6.9}$$

From matrix $\mathbf{A}^{-1}$, it is straightforward to compute its inverse, i.e. the matrix $\mathbf{A}$. We are mostly interested in the cases where inversion occurs owing to a change in pressure P given by the first column of $\mathbf{A}$. For instance, we look at conditions of the type $\mathcal{C}(\lambda \mid P) = A_{11} = 0$, which is the condition for an inversion of the radial strain under a change in pressure.

(b) A cylinder with equal fibres and equal and opposite orientations

We start our analysis with the simple case of a cylinder with two families of fibres of equal strength $(\mu_6 = \mu_4)$ and opposite orientation $(\Psi = \Phi)$ in the absence of fibre pre-compression $(\nu_1 = \nu_2 = 1)$. This corresponds to the classical case of the McKibben actuators, arteries and other hydrostats. Under extension or inflation, the couples created by the two fibres cancel out and there is no net

---

[4] We could have equivalently use the three loads (P, N, F) but all expressions are given in terms of F and not N.

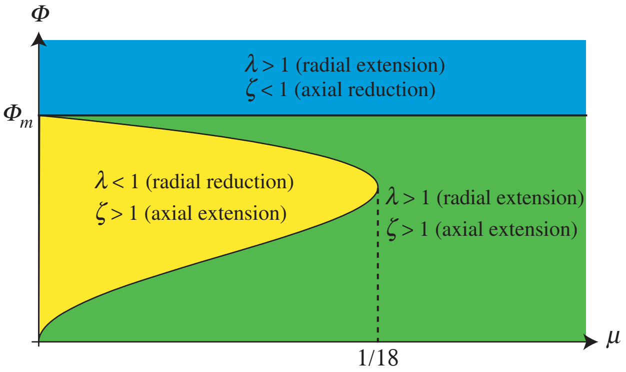

Figure 5. Parameter space for the radial and axial expansion of a thin tube under pressure. Depending on the relative stiffness of the fibre versus the matrix and the fibre angle, a capped tube under pressure can extend radially and axially (bottom-left), extend radially but shrink axially (top) or extend axially but shrink radially (bottom right). (Online version in colour.)

couple associated with the deformation and thus no rotation or twist ($\tau = 0$). In this particular case, the matrix A is given by

$$A = \begin{pmatrix} \dfrac{3\mu_1 + \mu_4 \sin^2(\Phi)(1 - 3\cos(2\Phi))}{2\mu_1(6\mu_1 + (3\cos(4\Phi) + 5)\mu_4)} & -\dfrac{\mu_4 \sin^2(2\Phi) + 2\mu_1}{4\pi\mu_1(6\mu_1 + (3\cos(4\Phi) + 5)\mu_4)} & 0 \\ \dfrac{\cos^2(\Phi)(3\cos(2\Phi) - 1)\mu_4}{2\mu_1(6\mu_1 + (3\cos(4\Phi) + 5)\mu_4)} & \dfrac{\mu_4 \cos^4(\Phi) + \mu_1}{\pi\mu_1(6\mu_1 + (3\cos(4\Phi) + 5)\mu_4)} & 0 \\ 0 & 0 & \dfrac{1}{2\pi\mu_4 \sin^2(2\Phi) + 2\pi\mu_1} \end{pmatrix}. \tag{6.10}$$

We are particularly interested in identifying inversion owing to internal change of pressure. This corresponds to the first column of the matrix above. The condition for an inversion of the radial strain is then $\mathcal{C}(\lambda \mid P) = A_{11} = 0$, that is

$$3\mu_1 + \mu_4 \sin^2(\Phi)(1 - 3\cos(2\Phi)) = 0. \tag{6.11}$$

The condition for an inversion in the axial strain, namely $\mathcal{C}(\zeta | P) = A_{21} = 0$, is

$$\Phi_\mathrm{m} = \tfrac{1}{2}\arccos(\tfrac{1}{3}) \approx 35.26440^\circ. \tag{6.12}$$

By denoting $\mu = \mu_1/\mu_4$ as the ratio of matrix modulus to the fibre modulus, we obtain a complete description of the possible inversions under a change in pressure in the parameter space (μ and Φ) as shown in figure 5.

The angle Φ_m is the magic angle discussed in the introduction and is well known in the theory of actuators, arteries and hydrostats [24,25,30,31,33,53]. Depending on the design criterion, one can consider different tube constructions by varying the fibre angle. For fibre angles larger than Φ_m, the tube contracts under increased pressure and this behaviour provides a model for pneumatic muscles. For tubes with fibre angle close to Φ_m, the deformation of the tube in the axial direction is minimal. For fibre angles less than Φ_m, the tube extends maximally. The magic angle Φ_m is also the particular angle found, by purely geometric arguments [23], by Clarke and Cowey in their theory of hydrostats. Note that this analysis is only valid for small enough P, for larger pressure, we expect the tube to increase eventually in length and radius.

(c) A cylinder with equal fibres and different orientations

Next, we consider the problem of rotation under pressure in a tube with two fibres with equal strength ($\mu_6 = \mu_4$) and no pre-compression ($\nu_1 = \nu_2 = 1$), but varying angle. If we freeze one fibre,

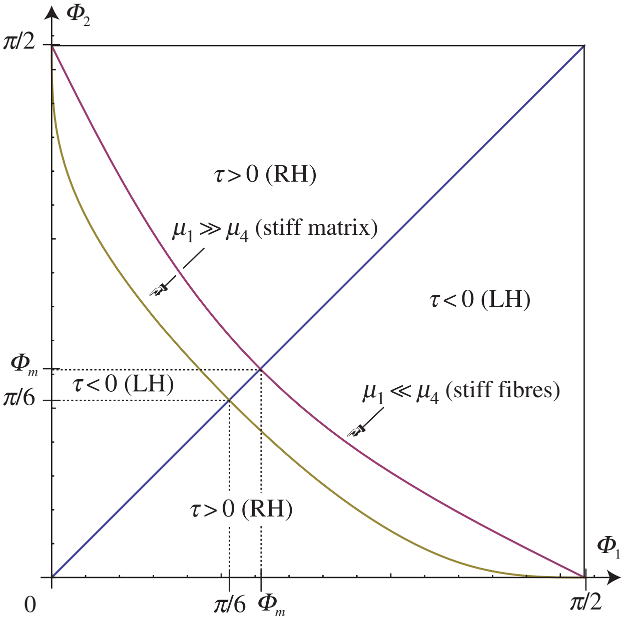

Figure 6. Twist induced by inflation for a cylindrical membrane in small deformation as a function of the orientation of the two fibres. RH, right-handed and LH, left-handed. (Online version in colour.)

we can vary the angle of the other fibre and ask whether a change in pressure will lead to a reversal in rotation from a left-handed rotation ($\tau < 0$, clockwise rotation viewed from above) to a right-handed rotation ($\tau > 0$, anti-clockwise rotation viewed from above). The condition for inversion is obtained from $\mathcal{C}(\tau \mid P) = A_{31} = 0$ and simplifies to

$$\mu_4 \sin(\Phi - \Psi)[6\mu_1(2\cos(\Phi + \Psi) + \cos(3\Phi + \Psi) + \cos(\Phi + 3\Psi)) \\ + 8\mu_4 \sin^2(\Phi + \Psi)(\cos(\Phi)\cos(\Psi) - 2\sin(\Phi)\sin(\Psi))] = 0. \tag{6.13}$$

We show in figure 6, the inversion curves in the parameter space (Φ, Ψ), for $\mu_1 \ll \mu_4$ and $\mu_4 \ll \mu_1$ (the two limits being easily obtained analytically from (6.13) by taking $\mu_1 = 0$ or $\mu_4 = 0$). Again we see the role of the magic angle as being the particular value at which an inversion of rotation appears for systems with stiff fibres. In this case, if we start with one fibre oriented at the magic angle and vary the other one, there will be just a single inversion of rotation (when the two are equal). For other values, there will be two inversions, one when the two angles are equal and the second at a different value of the angle, showing the interesting property of no net rotation (in small deformation) despite the tube being clearly anisotropic.

7. Inversions and perversions in the presence of pre-compression

All of the above analyses have been performed in the absence of pre-compression. When pre-compression is included, the problem is more involved because it results in a residually stressed system with non-zero strains, even in the absence of loads. This is due to the fact that there is a balance between stress in the fibres and stress in the matrix, and there is no configuration where both can be at rest. Therefore, the base state cannot be simply taken as the reference configuration. Despite these difficulties some simple cases can be analysed in some detail.

(a) A single fibre with pre-compression

Here, we consider the simplest non-trivial case of a tube with a single pre-compressed fibre. In this case, the strain-energy density can be obtained by setting $\mu_6 = 0$ in (2.17). We take, without loss of

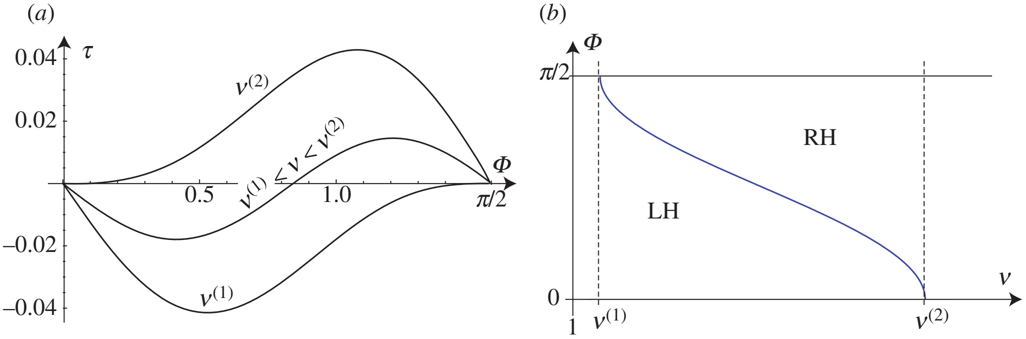

Figure 7. (a) The twist τ as a function of the fibre angle Φ for a capped cylinder under pressure with a single fibre in pre-compression. The particular case $P = 0.2$, $\mu_4 = 10$ is used. In this case, $\nu^{(1)} \approx 1.002082$ and $\nu^{(2)} \approx 1.05641$. ($b$) Generic change of twist as a function of the angle and the pre-compression. For $\nu < \nu^{(1)}$, the rotation is left-handed (negative τ) and right-handed for $\nu > \nu^{(2)}$. For $\nu^{(2)} < \nu < \nu^{(1)}$, the rotation can be left-handed or right-handed depending on the fibre angle. (Online version in colour.)

generality, $\mu_1 = 1$ and we are left with three material parameters (Φ, ν and μ_4) and one load P. We now ask the following question: does a capped tube with a single helical fibre $\Phi \in [0, \pi/2]$ under positive pressure P rotate clockwise (left-handed) or anti-clockwise? We start by considering the simple problem of twist for very small values of pre-compression as shown in figure 7a (curve $\nu^{(1)}$). As expected from the case with no pre-compression, a tube with right-handed helical fibre under pressure creates a left-handed rotation. Next, we consider the same system with increased values of the parameter ν. There, we observe that the rotation changes sign, that is, a perversion takes place. Ultimately for larger values of ν, the rotation is completely inverted, i.e. entirely right-handed rotation for all values of the fibre angle. Based on these observations, we are interested in identifying the precise values of P, ν and Φ for which a perversion occurs. To do so, we consider an initial state with $M = F = \tau = 0$ with an unknown initial pressure. The three equations (4.2)–(4.4) simplify to

$$\cos^2\Phi = \frac{\zeta^2 + \lambda^2 - \nu^2}{\zeta^2 - \lambda^2}, \quad 1 - 2\zeta^4\lambda^2 + \zeta^2\lambda^4 = 0 \quad \text{and} \quad \mu_1(\zeta^2\lambda^4 - 1) = P\zeta^3\lambda^4. \tag{7.1}$$

We can easily find the values of P and ν for which the perversion occurs at $\Phi = \pi/2$ and $\Phi = 0$, corresponding to the vales $\nu^{(1)}$ and $\nu^{(2)}$ in figure 7. For $\nu < \nu^{(1)}$, the rotation is left-handed and right-handed for $\nu > \nu^{(2)}$. For a given P, the first critical value $\nu^{(1)}$ is the first real root larger than 1 of

$$\nu^{5/2}(\nu^3 + \sqrt{8 + \nu^6})(P(\nu^3 + \sqrt{8 + \nu^6})^{1/2} - 2\sqrt{\nu}) + 8 = 0. \tag{7.2}$$

Similarly, for a given P, the second critical value $\nu^{(2)}$ is the first real root larger than 1 of

$$\nu^2 P^2 + 4(\nu^6 - 1)(\nu P - 1) = 0. \tag{7.3}$$

Note that perversion only occurs for the pressure values

$$P \le \frac{\sqrt[6]{(2/(13 + 3\sqrt{21}))}(2\sqrt{57 + 12\sqrt{21}} - 3(1 + \sqrt{21}))}{5^{5/6}} \approx 0.749868$$

which corresponds to a maximal axial stretch of $\zeta \approx 1.17819$. Note also that none of these values depend on the fibre strength μ_4. The possibility of a perversion is a rather surprising result. Indeed, it demonstrates that the chirality of the fibres does not necessarily determine the chirality of the cylindrical structure and its rotation, even for small values of pre-compression (less than 1%). In this range, the structure will exhibit macroscopic left-handed or right-handed rotation depending on the fibre angle, and small changes in the pre-compression and angle will change the rotation. This is indeed what is observed in the rotation of *Phycomyces* where new fibres are continuously laid down during growth. A new fibre that is added to the structure without pre-stress while the matrix is being stretched (in the current configuration) is equivalent to a pre-compressed fibre in the reference configuration. Despite the fibres being always observed as right-handed, the overall rotation of the sporangium can be either left-handed or right-handed depending on its growth stage [20].

8. Conclusion

Our study of fibre-reinforced tubes has shown that anisotropic elastic materials can exhibit non-intuitive behaviour under loads. For instance, a capped cylinder can either lengthen or increase in girth (or both) depending on both the fibre orientation and the relative stiffness of the matrix and fibres. A cylinder with clear anisotropy (having two families of fibres with equal strength but different orientation) may not exhibit any rotation when inflated. Finally, we showed that a tube with a single pre-compressed right-handed fibre may turn clockwise or anti-clockwise depending on the material parameters—clearly demonstrating that transfer of chirality from the microstructure (cell-wall anisotropy) to the macroscopic structure (the cell) depends both on geometry and mechanical response. This simple observation is typically not recognized in biology and physics as demonstrated for the case of helical springs in Goriely *et al*. [54].

These inversions of rotation are a particular class of behaviours that nonlinear continuum materials may exhibit. They can be understood as non-monotonous behaviour along either a loading or a remodelling path. Once the general framework for the onset of such behaviour is understood, it is not hard to identify other systems with similar features, e.g.

- the inflation of a spherical (or cylindrical) shell under controlled volume leads to a non-monotonous response of the pressure [55–57];
- the Poynting effect can be considered as an inversion of the normal displacement under pure shear tress (or, equivalently in torsion) [58,59];
- the inversion of the axial strain for pressurized arteries under fixed axial loads [34,60];
- the swelling or shrinking of a rectangular anisotropic elastic tissue with dispersed fibres under uniaxial tension: depending on the degree of dispersion of the fibres such a tissue will either shrink or swell in the direction perpendicular to the fibres (demonstrated numerically in [32]); and
- the inversion of rotation for a helical rod under a pure axial load [54].

Many of these behaviours are due to either a true nonlinear response of the material, to material anisotropy, or to coupling of anisotropy with a nonlinear response. For the past century there has been an emphasis on isotropic linear elastic systems where such non-monotonous responses are not expected and it is, therefore, not surprising that these phenomena appear counterintuitive. The approach described here can be used to identify many more inversions and perversions in mechanical and biological systems.

This publication is based on work supported in part by Award No. KUK-C1-013-04, made by King Abdullah University of Science and Technology (KAUST), and based in part upon work supported by the National Science Foundation under grants no. DMS-0907773 (M.T.). A.G. is a Wolfson Royal Society Merit Holder and acknowledges support from a Reintegration Grant under EC Framework VII.

References

1. Putz FE, Holbrook NM. 1991 The biology of climbing plants. In *Biomechanical studies of vines* (eds FE Putz, HA Mooney). Cambridge, UK: Cambridge University Press.

2. Silk WK, Holbrook NM. 2005 The importance of frictional interactions in maintaining the stability of the twining habit. *Am. J. Bot.* **92**, 1820–1826. (doi:10.3732/ajb.92.11.1820)
3. Schulgasser K, Witztum A. 2006 The mechanism of spiral grain formation in trees. *Wood Sci. Technol.* **41**, 133–156. (doi:10.1007/s00226-006-0100-y)
4. Fournier M, Bordonne PA, Guitard D, Okuyama T. 1990 Growth stress patterns in tree stems. *Wood Sci. Technol.* **24**, 131–142. (doi:10.1007/BF00229049)
5. Goriely A, Tabor M. 2003 Biomechanical models of hyphal growth in actinomycetes. *J. Theor. Biol.* **222**, 211–218. (doi:10.1016/S0022-5193(03)00029-8)
6. Koch AL. 1994 The problem of hyphal growth in streptomycetes and fungi. *J. Theor. Biol.* **171**, 137–150. (doi:10.1006/jtbi.1994.1219)
7. The Society for Actinomycetes Japan. 1997 *Atlas of Actinomycetes*. Tokyo, Japan: Asakura Publishing Co. ltd.
8. Jones LJF, Carballido-Lopez R, Errington J. 2001 Control of cell shape in bacteria: helical, actin-like filaments in *Bacillus subtilis*. *Cell* **104**, 913–922. (doi:10.1016/S0092-8674(01)00287-2)
9. Mendelson NH. 1978 Helical *Bacillus subtilis* macrofibers: morphogenesis of a bacterial multicellular macroorganism. *Proc. Natl Acad. Sci. USA* **75**, 2478–2482. (doi:10.1073/pnas.75.5.2478)
10. Mendelson NH. 1999 *Bacillus subtilis* macrofibers, colonies and bioconvection patterns use different strategies to achieve multicellular organization. *Environ. Microbiol.* **1**, 471–477. (doi:10.1046/j.1462-2920.1999.00066.x)
11. Howard RJ, Valent B. 1996 Breaking and entering: host penetration by the fungal rice blast pathogen, *Magnaporthe grisea*. *Annu. Rev. Microbiol.* **50**, 491–512. (doi:10.1146/annurev.micro.50.1.491)
12. Talbot NJ. 2003 On the trail of a cereal killer: exploring the biology of *Magnaporthe grisea*. *Annu. Rev. Microbiol.* **57**, 177–202. (doi:10.1146/annurev.micro.57.030502.090957)
13. Tongen A, Goriely A, Tabor M. 2006 Biomechanical model for appressorial design in *Magnaporthe grisea*. *J. Theor. Biol.* **240**, 1–8. (doi:10.1016/j.jtbi.2005.08.014)
14. Castle ES. 1942 Spiral growth and reversal of spiraling in *Phycomyces*, and their bearing on primary wall structure. *Am. J. Bot.* **29**, 664–672. (doi:10.2307/2437180)
15. Cohen R, Delbrück M. 1958 Distribution of stretch and twist along the growing zone of the sporangiophore of phycomyces and the distribution of response to a periodic illumination program. *J. Cell Comp. Physiol.* **52**, 361–388. (doi:10.1002/jcp.1030520303)
16. Oort AJP. 1931 The spiral growth of phycomyces. *Proc. R. Soc. Lond. A* **34**, 564.
17. Ortega JKE, Gamow RI. 1974 The problem of handedness reversal during the spiral growth of phycomyces. *J. Theor. Biol.* **47**, 317–332. (doi:10.1016/0022-5193(74)90201-X)
18. Preston RD. 1948 Spiral growth and spiral structure I. Spiral growth in sporangiophores of phycomyces. *Biochim. Biophys. Acta* **2**, 155–166. (doi:10.1016/0006-3002(48)90024-9)
19. Roelofsen PA. 1950 The origin of spiral growth in *Phycomyces* sporangiophores. *Recueil Trav. Bot. Neerl.* **42**, 72–110.
20. Goriely A, Tabor M. 2011 Spontaneous rotational inversion in *Phycomyces*. *Phys. Rev. Lett.* **106**, 138103. (doi:10.1103/PhysRevLett.106.138103)
21. Wold MP, Gamow RI. 1992 Fiber-composite model for helical growth in the Phycomyces cell wall. *J. Theor. Biol.* **159**, 39–51. (doi:10.1016/S0022-5193(05)80766-0)
22. Harris JE, Crofton HD. 1957 Structure and function in the nematodes: internal pressure and cuticular structure in ascaris. *J. Exp. Biol.* **34**, 116–130.
23. Clark RB, Cowey JB. 1958 Factors controlling the change of shape of certain nemertean and turbellarian worms. *J. Exp. Biol.* **35**, 731–748.
24. Kier WM. 2012 The diversity of hydrostatic skeletons. *J. Exp. Biol.* **215**, 1247–1257. (doi:10.1242/jeb.056549)
25. Kier WM, Smith KK. 1985 Tongues, tentacles and trunks: the biomechanics of movement in muscular-hydrostats. *Zool. J. Linn. Soc.* **83**, 307–324. (doi:10.1111/j.1096-3642.1985.tb01178.x)
26. McCurley RS, Kier WM. 1995 The functional morphology of starfish tube feet: the role of a crossed-fiber helical array in movement. *Biol. Bull.* **188**, 197–209. (doi:10.2307/1542085)
27. Adams DS, Keller R, Koehl MA. 1990 The mechanics of notochord elongation, straightening and stiffening in the embryo of *Xenopus laevis*. *Development* **110**, 115–130.
28. Koehl MAR. 2003 Physical modelling in biomechanics. *Phil. Trans. R. Soc. Lond. B* **358**, 1589–1596. (doi:10.1098/rstb.2003.1350)
29. Koehl MAR, Quillin KJ, Pell CA. 2000 Mechanical design of fiber-wound hydraulic skeletons: the stiffening and straightening of embryonic notochords. *Am. Zool.* **40**, 28–41. (doi:10.1668/0003-1569(2000)040[0028:MDOFWH]2.0.CO;2)

30. Daerden F, Lefeber D. 2002 Pneumatic artificial muscles: actuators for robotics and automation. *Eur. J. Mech. Environ. Eng.* **47**, 11–21.
31. Liu W, Rahn CR. 2003 Fiber-reinforced membrane models of Mckibben actuators. *J. App. Mech.* **70**, 853–859. (doi:10.1115/1.1630812)
32. Holzapfel GA, Ogden RW. 2010 Constitutive modelling of arteries. *Proc. R. Soc. A* **466**, 1551–1597. (doi:10.1098/rspa.2010.0058)
33. Holzapfel GA, Gasser TC. 2001 A viscoelastic model for fiber-reinforced composites at finite strains: continuum basis, computational aspects and applications. *Comp. Methods Appl. Mech. Eng.* **190**, 4379–4403. (doi:10.1016/S0045-7825(00)00323-6)
34. Holzapfel GA, Gasser TC, Ogden RW. 2000 A new constitutive framework for arterial wall mechanics and a comparative study of material models. *J. Elast.* **61**, 1–48. (doi:10.1023/A:1010835316564)
35. Goriely A, Tabor M. 1998 Spontaneous helix-hand reversal and tendril perversion in climbing plants. *Phys. Rev. Lett.* **80**, 1564–1567. (doi:10.1103/PhysRevLett.80.1564)
36. Listing JB. 1847 Vorstudien über topologie. *Göttinger Studien* **1**, 811–875.
37. Maxwell JC. 1892 *A treatise on electricity and magnetism*. Oxford, UK: Clarendon.
38. McMillen T, Goriely A. 2002 Tendril perversion in intrinsically curved rods. *J. Nonlinear Sci.* **12**, 241–281. (doi:10.1007/s00332-002-0493-1)
39. Ogden RW. 1984 *Non-linear elastic deformation*. New York, NY: Dover.
40. Adkins JE, Rivlin RS. 1955 Large elastic deformations of isotropic materials X. Reinforcement by inextensible cords. *Phil. Trans. R. Soc. Lond. A* **248**, 201–223. (doi:10.1098/rsta.1955.0014)
41. Spencer AJM. 1972 *Deformations of fiber-reinforced materials*. Oxford, UK: Clarendon Press.
42. Triantafyllidis N, Abeyaratne R. 1983 Instabilities of a finitely deformed fiber-reinforced elastic material. *J. Appl. Mech.* **50**, 149. (doi:10.1115/1.3166983)
43. Merodio J, Ogden RW. 2003 Instabilities and loss of ellipticity in fiber-reinforced compressible non-linearly elastic solids under plane deformation. *Int. J. Solids Struct.* **40**, 4707–4727. (doi:10.1016/S0020-7683(03)00309-3)
44. Merodio J, Ogden RW. 2005 Mechanical response of fiber-reinforced incompressible non-linearly elastic solids. *Int. J. Nonlinear Mech.* **40**, 213–227. (doi:10.1016/j.ijnonlinmec.2004.05.003)
45. Horgan CO, Murphy JG. 2011 Torsion of incompressible fiber-reinforced nonlinearly elastic circular cylinders. *J. Elast.* **103**, 235–246. (doi:10.1007/s10659-010-9282-5)
46. Saccomandi G. 2001 Universal results in finite elasticity. *Nonlinear Elast. Theor. Appl.* **283**, 97–134. (doi:10.1017/CBO9780511526466.004)
47. Qiu GY, Pence TJ. 1997 Remarks on the behavior of simple directionally reinforced incompressible nonlinearly elastic solids. *J. Elast.* **49**, 1–30. (doi:10.1023/A:1007410321319)
48. Demirkoparan H, Pence TJ. 2008 Torsional swelling of a hyperelastic tube with helically wound reinforcement. *J. Elast.* **92**, 61–90. (doi:10.1007/s10659-007-9149-6)
49. Merodio J, Ogden RW. 2006 The influence of the invariant I8 on the stress-deformation and ellipticity characteristics of doubly fiber-reinforced non-linearly elastic solids. *Int. J. Nonlinear Mech.* **41**, 556–563. (doi:10.1016/j.ijnonlinmec.2006.02.001)
50. Pence TJ, Wineman A. 2012 On some connections between equivalent single material and mixture theory models for fiber reinforced hyperelastic materials. *Int. J. Nonlinear Mech.* **47**, 285–292. (doi:10.1016/j.ijnonlinmec.2011.06.011)
51. Rivlin RS. 1948 Large elastic deformations of isotropic materials. III. Some simple problems in cylindrical polar co-ordinates. *Phil. Trans. R. Soc. Lond. A* **240**, 509–525. (doi:10.1098/rsta.1948.0004)
52. Rivlin RS. 1948 Large elastic deformations of isotropic materials. IV. Further developments of the general theory. *Phil. Trans. R. Soc. Lond. A* **241**, 379–397. (doi:10.1098/rsta.1948.0024)
53. Santulli C, Patel SI, Jeronimidis G, Davis FJ, Mitchell GR. 2005 Development of smart variable stiffness actuators using polymer hydrogels. *Smart Mater. Struct.* **14**, 434. (doi:10.1088/0964-1726/14/2/018)
54. Goriely A, Maddocks JH, Durickovic B. 2012 Twist and stretch of helices: all you need is Love. Preprint [13/11], Oxford Center for Collaborative Applied Mathematics. Available on request.
55. Chen YC, Haughton DM. 2003 Stability and bifurcation of inflation of elastic cylinders. *Proc. R. Soc. Lond. A* **459**, 137–156. (doi:10.1098/rspa.2002.1024)
56. Ben Amar M, Goriely A. 2005 Growth and instability in elastic tissues. *J. Mech. Phys. Solids* **53**, 2284–2319. (doi:10.1016/j.jmps.2005.04.008)

57. Horny L, Kronek J, Chlup H, Gultova E, Heller L, Zitny R, Vokoun D. 2012 Inflation-extension test of silicon rubber-nitinol composite tube. In *5th European Conf. of the International Federation for Medical and Biological Engineering, Budapest, Hungary, 14–18 September 2011*, pp. 1027–1030. Berlin, Germany: Springer.
58. Mihai LA, Goriely A. 2011 Positive or negative poynting effect? the role of adscititious inequalities in hyperelastic materials. *Proc. R. Soc. A* **467**, 3633–3646. (doi:10.1098/rspa.2011.0281)
59. Mihai LA, Goriely A. 2012 Numerical simulation of shear and the poynting effects by the finite element method: an application of the generalised empirical inequalities in non-linear elasticity. *Int. J. Non-Linear Mech.* **49**, 1–14. (doi:10.1016/j.ijnonlinmec.2012.09.001)
60. Gasser TC, Ogden RW, Holzapfel GA. 2006 Hyperelastic modelling of arterial layers with distributed collagen fiber orientations. *J. R. Soc. Interface* **3**, 15–35. (doi:10.1098/rsif.2005.0073)